Supplementary Information (SI) for Journal of Materials Chemistry A.

Supporting Information

Dynamic Hydrogen Bond Evolution in Thermosensitive Hydrogels for Self-Adaptive Passive Cooling

Sijia Ge,[1,2#] Ning Yang,[3#] Xiaoyue Zhu,[4#] Xiaoyu Min,[2] Ying Kong,[1] Changshun Xu,[2]
Hong Yang,*[5✉] Jin Wang,*[1,2✉]

1 Key Laboratory of Multifunctional Nanomaterials and Smart Systems, Suzhou Institute of Nano-Tech and Nano-Bionics, Chinese Academy of Sciences, Suzhou 215123, China. *E-mail: jwang2014@sinano.ac.cn.

2 School of Nano-Tech and Nano-Bionics, University of Science and Technology of China, Hefei 230026, China

3 College of Basic Medicine, Zunyi Medical University, Zunyi, 563099, China

4 Department of Otolaryngology Head and Neck Surgery, Shanghai Key Laboratory of Sleep Disordered Breathing, Shanghai Sixth People's Hospital Affiliated to Shanghai Jiao Tong University School of Medicine, Shanghai, 200233, China

5 School of Chemistry and Chemical Engineering, State Key Laboratory of Digital Medical Engineering, Southeast University, Nanjing, Jiangsu Province 211189, P.R. China. yangh@seu.edu.cn

[#]These authors contribute equally

EXPERIMENTAL SECTION

Characterization.

Scanning electron microscope (SEM) analysis. The morphology of the samples was observed by a FEI Quanta FEG 250 scanning electron microscope at accelerated electron energy of 5.0 kV. Test specimens were cryo-frozen in liquid nitrogen for 5 minutes, followed by freeze-drying and then the samples were taken for cross-sectional and planar observation. Test specimens at different temperatures were maintained at constant temperatures in water for 30 minutes, rapidly frozen with liquid nitrogen, then freeze-dried before morphological observation. The cross-sections of the specimens were coated with gold by a sputter coater for 20 seconds before measurement

Measurement of mechanical properties. All mechanical properties of the samples were tested on Instron 3365 electronic universal testing machine equipped with pneumatic clamps (QTS-600) at room temperature. The samples with a thickness of 0.5 mm were cut into rectangles (20 mm*5 mm). The rate of extension was fixed at 50 mm min^{-1} for tensile test test. After the hydrogels were stabilized in water at different temperatures, they were quickly stretched to test the mechanical properties of hydrogels at different temperatures.

UV/Vis spectroscopy. The hydrogel sample was directly synthesized in the UV-vis cell prior to the test. The transmittance curves of the P(NAGA-CO-NIPAm) hydrogels were built by turbidity measurement to collect the transmittance in the 300-900 nm wavelength range with a scanning rate of 0.1°C min^{-1} from 10 to 65 °C using a Pramodar P-7 spectrophotometer equipped with a A-1000 temperature controller (±0.1°C).

Dynamic mechanical analysis (DMA). The storage moduli and loss moduli of the hydrogel samples (cylinders, 10 mm in diameter and 4 mm in height) were measured using compression mode on a NETZSCH. Dynamic Mechanical Analyzer tests were carried out at 0-80°C at 2°C/min at constant frequency of 10 rad/s and 4% strain.

In situ variable-temperature FTIR spectroscopy. The in situ variable-temperature FTIR spectroscopy was performed on the P(NAGA-co-NIPAm)-4* hydrogel. A small aliquot of the equilibrated hydrogel was directly placed on the diamond crystal of an ATR-FTIR accessory integrated with a programmable temperature cell. The sample chamber was purged with dry nitrogen. Spectra were collected in a heating sequence from 10 to 45°C, specifically at setpoints of 10, 15, 25, 35, and 45°C. At each target temperature, the system was allowed to equilibrate for 5 minutes prior to acquiring the spectrum. The spectral changes, particularly in the N-H (3000-3600 cm^{-1}) and Amide I/II (1400-1700 cm^{-1}) regions, were monitored to analyze the evolution of hydrogen bonding and the phase transition behavior of the copolymer network as a function of temperature.

Determination of equilibrium water contents (EWCs). The EWCs of the hydrogels were measured at different temperature using a gravimetric method. The hydrogel samples were fully swollen in the deionized water. Then they were taken out, gently wiped with filter paper, and immediately weighed on a microbalance. Afterwards, the hydrogels were dried in a vacuum oven at 60 ºC until a constant weight as the dry weight of the hydrogel was obtained. The EWC is defined as the following Equation 1.

$$EWC = \frac{m_{wet}\text{-m}_{dry}}{\text{m}_{dry}} \qquad (1)$$

Where m_{wet} is the wet weight at different temperatures and m_{dry} is the dry weight of each sample. The average values and errors were calculated from at least four independent data for each specimen.

Differential Scanning Calorimetry (DSC). The phase transition of hydrogels was investigated by differential scanning calorimetry using a DSC Q200 from TA instrument. Hydrogels at preparation state (ca. 10 mg) were submitted to temperature cycles between 0 and 80°C under nitrogen atmosphere. The heating and cooling rates were fixed at 2°C min^{-1}.

Temperature and solar radiation monitoring. Temperature monitoring is carried out by Jinko JK808 handheld multi-channel temperature tester. Solar radiation monitoring using TES-1333/1333R solar power meter irradiator for monitoring.

Evaporative cooling efficiency test. The hydrogel was subjected to evaporative cooling at low (5°C), room (25°C) and high (45°C) temperatures for 1h, weighed the weight lost and calculated to obtain its evaporative cooling efficiency, the results are shown in **Table S2**.

Maxwell Diffusion Modeling. The Maxwell diffusion model under stationary or low velocity airflow conditions is formulated as：

$$J = \mathrm{D.M}\frac{\left(P_{sat} - P_{\infty}\right)}{RT\delta} \qquad （2）$$

where D is the diffusion coefficient of water vapor in air, M is the molar mass of water, P_{sat} is the saturation vapor pressure of water, P_{∞} is the ambient water vapor partial pressure, R is the gas constant, T is the temperature, and δ is the thickness of the boundary layer.

The diffusion coefficients of water at water at 5, 20 and 45°C were 2.42×10^{-5} m^2/s, 2.82×10^{-5} m^2/s and 3.61×10^{-5} m^2/s; the molar mass of water is 0.018 kg/mol; the saturated vapor pressure Psat of water at 5, 20, and 45°C is 0.5668 kPa, 2.338 kPa, and 9.58 kPa, respectively; the ambient partial pressure of water vapor, P∞, is dependent on the relative humidity, RH, e.g., P∞=0.5×Psat for RH=50%, and the RH inside the test chamber is 65%; the gas constant R is 8.314 J-mol^{-1}-K^{-1}; the temperature T is 318 K; δ is calculated as 1 mm to obtain the evaporation rate of water at different temperatures. The results of the calculation are shown in **Table S11** and the calculation process is as follows:

$$J_5 = \frac{2.02\times10^{-5}\times0.018\times(566.8-0.65\times566.8)}{8.314\times318\times0.001}\times3600 = 0.18$$

$$J_{20} = \frac{2.42\times10^{-5}\times0.018\times(3169-0.65\times3169)}{8.314\times318\times0.001}\times3600 = 0.71$$

$$J_{45} = \frac{2.82\times10^{-5}\times0.018\times(9580-0.65\times9580)}{8.314\times318\times0.001}\times3600 = 2.32$$

Derivation of Maxwell's diffusion model. Fick's law describes the relationship between the flux of matter J (mass passing through a unit area per unit time) and the concentration gradient during diffusion:

$$J = -D(\frac{dC}{dx}) \qquad (3)$$

where J is the diffusive flux ($kg\cdot m^{-2}\cdot s^{-1}$), D is the diffusion coefficient (m^2/s), and dC/dx is the concentration gradient ($kg\cdot m^{-4}$).

For the evaporation process, water vapor diffuses from the surface of the liquid (high concentration C_{sat}) to the surrounding air (low concentration C_∞), thus:

$$J = D(C_{sat} - C_\infty)/\delta \qquad (4)$$

where δ is the thickness of the diffuse boundary layer (m), indicating the area of significant concentration change.

According to the ideal gas equation of state, the gas concentration C (kg/m^3) is related to the partial pressure P (Pa):

$$C = \frac{RM}{TP} \qquad (5)$$

where M is the molar mass of water vapor (kg/mol), R is the universal gas constant (8.314 $J\cdot mol^{-1}\cdot K^{-1}$), and T is the absolute temperature (K).

Maxwell's diffusion model was obtained by replacing concentration with vapor pressure.

Calculation of hydrogen bond energy.

Molecular modeling was performed using GaussView 5.0. Geometric optimization and Gibbs free energy calculations were conducted at the B3LYP-D3/6-311G level of theory with Gaussian 09. Solvation effects were incorporated via the integral equation formalism polarizable continuum model (IEFPCM) using water as the solvent. The hydrogen bond energy was calculated as:

$$E_{\mathrm{HB}} = E_{\mathrm{A\text{-}G1d}} + E_{\mathrm{A\text{-}G1}} - E_{\mathrm{A}}$$

where $E_{\mathrm{A\text{-}G1d}}$ and $E_{\mathrm{A\text{-}G1}}$ represent the energies of molecule 1 and molecule 2, respectively, E_{A} represents the overall energy of the two molecules combined, and E_{HB} is the energy required for the spontaneous combination of the two molecules, i.e., the energy of the hydrogen bond.

Model development and statistical analysis

The weight of NAGA, weight of NIPAm, temperature and wavelength were used as inputs for the light transmittance of adaptive temperature-sensitive hydrogel prediction models. Two machine learning algorithms (light gradient boosting machine (LGB) and random forest (RF)), and linear regression model were constructed and compared. LGB algorithm obtains the suboptimal solution for split features and cut-off points through a histogram algorithm. It is an improved algorithmic framework based on gradient-boosted decision trees, characterized by fast training speed and high parallelism. RF is an ensemble learning algorithm consisting of multiple decision trees. It is not prone to overfitting, offers high accuracy, and exhibits excellent performance in both classification and regression tasks. The dataset was randomly split into a training set with 80% of the samples and a testing set with the remaining 20%. The testing set was used to evaluate the generalization ability of models. An evaluation was conducted on the three models in terms of the errors between their predictions and actual values, as well as their consistency. Descriptive statistics were used with mean ± standard deviations (SD). A paired t-test was used to compare the differences in light transmittance evaluated by the two methods. The mean squared error (MSE), mean absolute error (MAE) and coefficient of determination (R^2) were compared among three algorithms. Root mean squared error (RMSE) corresponding to the two methods, their ratio, and the Pearson correlation coefficient were calculated. A larger RMSE indicates a greater difference between the measured values and the predicted values. The intraclass correlation coefficient (ICC) and Bland-Altman analysis were employed to assess the consistency between the two methods. If $ICC > 0.90$, it indicates excellent consistency; $0.75 \leq ICC \leq 0.9$ indicates good consistency; $0.5 \leq ICC < 0.75$ indicates moderate consistency; and when $ICC < 0.5$, it indicates poor consistency. A Bland-Altman analysis was performed on the research data to calculate the limits of agreement (LoA) for the differences between the actual measurement method and the model prediction method. Machine learning library in Python was applied, such as ‘scikit-learn’, and ‘lightgbm’. ‘Gradio’ from Python was used for the interactive interface of model deployment and visualization. All statistical analyses and model developments were performed with R software (version 4.1.1) and Python (version 3.8.0). Two-sided P-values < 0.05 were considered as statistically significant.

Model deployment

The visualization of the light transmittance prediction model for adaptive temperature-sensitive hydrogel with the RF algorithm provided the possibility and convenience for predicting the light transmittance of adaptive temperature-sensitive hydrogel. Local servers of the model were deployed for use, and the interface was presented in **Figure. S4**. The Figure shows the sample for which the light transmittance of adaptive temperature-sensitive hydrogel was predicted when relevant values were imputed. The output presents the predicted light transmittance value. This prediction tool enables the possibility and convenience for predicting the light transmittance of adaptive temperature-sensitive hydrogel.

Table S1 Preparation of P(NAGA-CO-NIPAm) with different monomer ratios

Sample	NAGA (g)	NIPAm (g)	Bis (mg)	H_2O (μL)	NAGA：NIPAm
P(NAGA-CO-NIPAm)-1	0.14	0.26	2	750	7：13
P(NAGA-CO-NIPAm)-2	0.16	0.24	2	750	8：12
P(NAGA-CO-NIPAm)-3	0.18	0.22	2	750	9：11
P(NAGA-CO-NIPAm)-4	0.2	0.20	2	750	10：10
P(NAGA-CO-NIPAm)-5	0.22	0.18	2	750	11：9
P(NAGA-CO-NIPAm)-4*	0.19	0.21	2	750	19：21

Table S2 Predicted ratio of P(NAGA-CO-NIPAm) hydrogels

Sample	NAGA (g)	NIPAm (g)	Bis (mg)	H_2O (μL)
P(NAGA-CO-NIPAm)-P1	0.15	0.25	2	750
P(NAGA-CO-NIPAm)-P2	0.17	0.23	2	750
P(NAGA-CO-NIPAm)-P3	0.19	0.21	2	750

Table 3 The Performance of Machine Learning Models and Linear Regression in Predicting Light Transmittance of Adaptive Temperature-sensitive Hydrogel

Models	Mean squared error (MSE)	Mean absolute error (MAE)	Coefficient of Determination (R^2)
Random Forest	0.007	0.043	1.000
LightGBM	11.715	2.407	0.990
Linear Regression	168.190	10.970	0.860

Table 4 Comparison of Random Forest-Based Machine Learning Model Predictions and Measured Values for Light Transmittance

Models	Mean squared error (MSE)	Mean absolute error (MAE)	Coefficient of Determination (R^2)
Random Forest	0.007	0.043	1.000
LightGBM	11.715	2.407	0.990
Linear Regression	168.190	10.970	0.860

RMSE: root mean squared error; a. p-value of paired t-test; b. The corresponding P-value < 0.001.

Table 5 Consistency Analysis Between Random Forest Model Predictions and Measured Values for Light Transmittance

Characteristic	ICC (95%CI)	Predicted value(%) -Measured value (%)	BIA/APE	LoA	
				LLoA	ULoA
Wavelength % (mean±SD)	1.000 (1.000, 1.000)	0.018 (%)	1.000	-0.133 (-0.137, -0.129)	0.172 (0.168, 0.176)

ICC: intra-class correlation coefficient; LoA: limits of agreement; LLoA：low limits of agreement; ULoA：up limits of agreement.

Table S6: Comparison of Random Forest-Based Machine Learning Model Predictions and Measured Values for Light Transmittance in External Validation of Prospective Prediction

Characteristic	Predicted value (%)	Measured value (%)	t	Pa	rb	RMSE
Light Transmittance (mean±SD)	50.183±23.295	50.087±23.017	1.286	0.199	0.963	6.311

RMSE: root mean squared error;

a. p-value of paired t-test;

b. The corresponding P-value < 0.001.

Table S7: The main types of hydrogen bonds and corresponding hydrogen bond energies of P(NAGA-CO-NIPAm)-4* hydrogel at 5°C.

	5°C	
Hydrogen-bonded structure	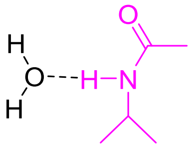	
Molecular energy	G（ Hartree）	Interaction energy (hydrogen bonding energy)（kcal/mol）
A	-403.379245	
A-G1	-76.414426	
A-G1d	-326.969891	-3.19536
Hydrogen-bonded structure	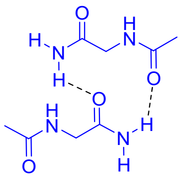	
Molecular energy	G（ Hartree）	Interaction energy (hydrogen bonding energy)（kcal/mol）
B	-834.17818	
B-G1	-417.09208	
B-G1d	-417.091545	-3.43035

Table S8: The main types of hydrogen bonds and corresponding hydrogen bond energies of P(NAGA-CO-NIPAm)-4* hydrogel at 30°C.

30℃		
Hydrogen-bonded structure	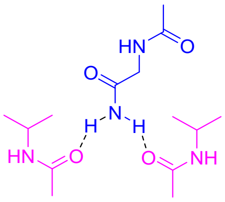	
Molecular energy	G（ Hartree）	Interaction energy (hydrogen bonding energy)（kcal/mol）
B	-1071.033851	
B-G1	-326.973398	
B-G1d	-744.064857	-2.77452
B	-1071.033851	
B-G2	-326.973409	
B-G2d	-744.062006	-0.98532
Hydrogen-bonded structure	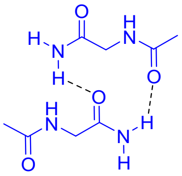	
Molecular energy	G（ Hartree）	Interaction energy (hydrogen bonding energy)（kcal/mol）
D	-834.18383	
D-G1	-417.095862	
D-G1d	-417.095253	-4.58955

Table S9: The main types of hydrogen bonds and corresponding hydrogen bond energies of P(NAGA-CO-NIPAm)-4* hydrogel at 45°C.

45°C		
Hydrogen-bonded structure	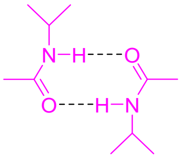	
Molecular energy	G（ Hartree）	Interaction energy (hydrogen bonding energy)（kcal/mol）
A	-653.948172	
A-G1	-326.975589	
A-G1d	-326.975589	-1.89378
Hydrogen-bonded structure	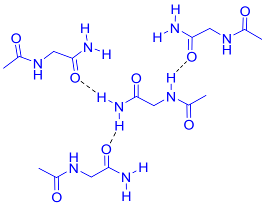	
Molecular energy	G（ Hartree）	Interaction energy (hydrogen bonding energy)（kcal/mol）
B	-1668.377344	
B-G1	-417.097943	
B-G1d	-1251.281818	-1.52271
B	-1668.377344	
B-G2	-417.097511	
B-G2d	-1251.28474	-3.09141
B	-1668.377344	
B-G3	-417.097511	
B-G3d	-1251.284823	-3.1437

Table S10: Evaporation efficiency of P(NAGA-CO-NIPAm)-4*, PNIPAm, and PNAGA hydrogel in SuZhou

Temperatures(°C) Samples	5	25	45
P(NAGA-CO-NIPAm)-4*	0.035 kg/(m^2.h) or 21.97 W/m^2	0.086 kg/(m^2.h) or 53.99 W/m^2	0.97 kg/(m^2.h) or 608.94 W/m^2
PNAGA	0.032 kg/(m^2.h) or 20.01 W/m^2	0.052 kg/(m^2.h) or 32.64 W/m^2	0.42 kg/(m^2.h) or 263.67 W/m^2
PNIPAm	0.054 kg/(m^2.h) or 33.90 W/m^2	0.15 kg/(m^2.h) or 94.17 W/m^2	2.31 kg/(m^2.h) or 1450.17 W/m^2

Table S11: Theoretical evaporation rate of water

Temperatures(°C) Samples	5	25	45
H_2O	0.18 kg/(m^2.h) or 113 W/m^2	0.71 kg/(m^2.h) or 445.72 W/m^2	2.32 kg/(m^2.h) or 1456.44 W/m^2

Table S12 A comparative study on the cooling performance of recent hydrogel passive cooling materials

Number	Material System	Low cooling capacity（W/m^2）	High cooling capacity（W/m^2）	Maximum temperature reduction（℃）	Cooling duration（h）	Ref
1	PVA/PVP/PEG composite hydrogel	77.8	234.24	18.9	24	45
2	Lotus root starch hydrogel	272	464	23.5	2.5	46
3	PNIPAm hydrogel	/	1250	13	3	47
4	Polyvinyl alcohol hydrogel	100	213.5	8.7	9	48
5	HPC/CaCl$_2$ Hydrogel	/	109.3	12.3	/	49
6	HPC hydrogel	103	136.9	9.2	5	50

7	PVA hydrogel	65	273	9.37	3	51
8	PAAm/PVA hydrogel	138	233	6.2	1	52
9	PVA composite hydrogel	43	201	14.7	9	12
10	PAAS hydrogel	**76**	190	7.2	9	3
11	P(NAGA-CO-NIPAm)-4*	21.97	608.94	17.44	144	This work

List of Abbreviations: Polyvinyl alcohol (PVA), Polyvinylpyrrolidone (PVP), Polyethylene glycol (PEG), Polyacrylamide (PAm), Sodium polyacrylate(PAAS), Hydroxypropyl cellulose (HPC).

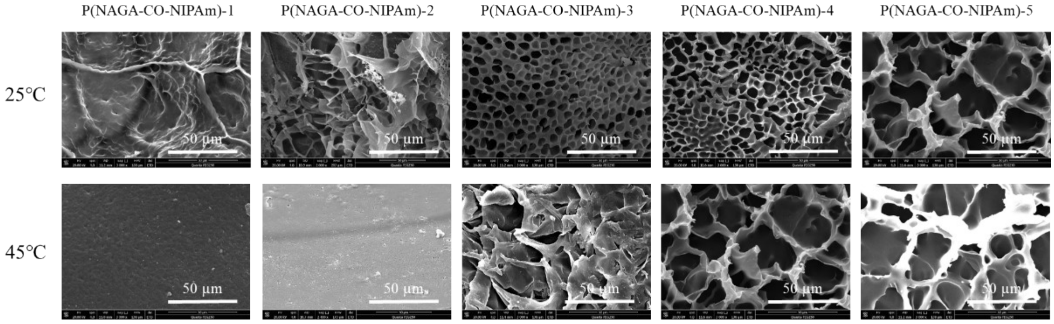

Figure. S1. SEM of P(NAGA-CO-NIPAm) at 25 °C and 45 °C.

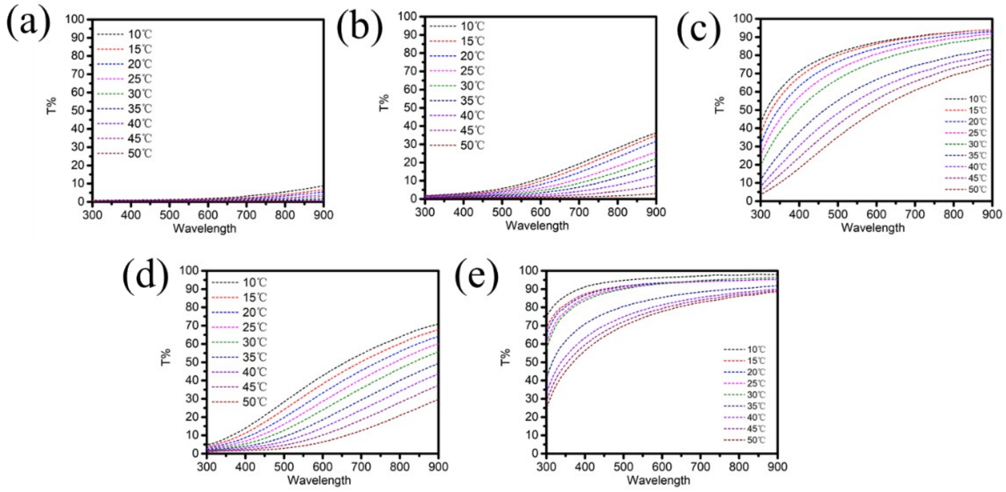

Figure. S2. Transmittance of (a) P(NAGA-CO-NIPAm)-1, (b) P(NAGA-CO-NIPAm)-2, (c) P(NAGA-CO-NIPAm)-3, (d) P(NAGA-CO-NIPAm)-4 and (e) P(NAGA-CO-NIPAm)-5.

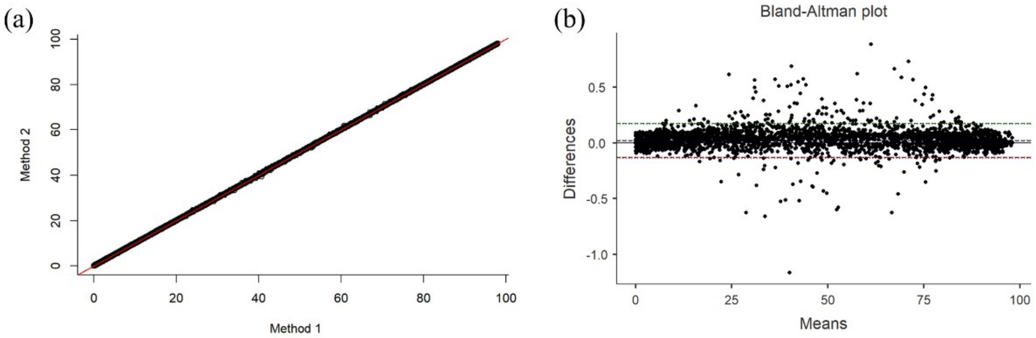

Figure. S3. (a) Plot of Predictions Value and Measured Value with Line of Equality (Method 1: Random Forest-Based Machine Learning Model Predictions; Method 2: Measured Values.); (b) Bland-Altman Plot.

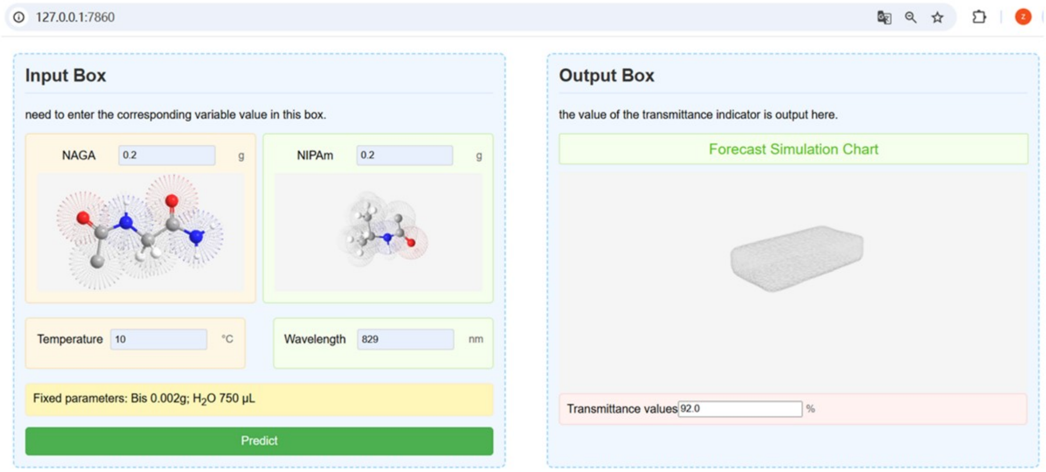

Input Box

need to enter the corresponding variable value in this box.

NAGA 0.2 g

NIPAm 0.2 g

Temperature 10 °C

Wavelength 829 nm

Fixed parameters: Bis 0.002g; H_2O 750 μL

Output Box

the value of the transmittance indicator is output here.

Transmittance values 92.0 %

Figure. S4. Prediction interface for hydrogel transmittance.

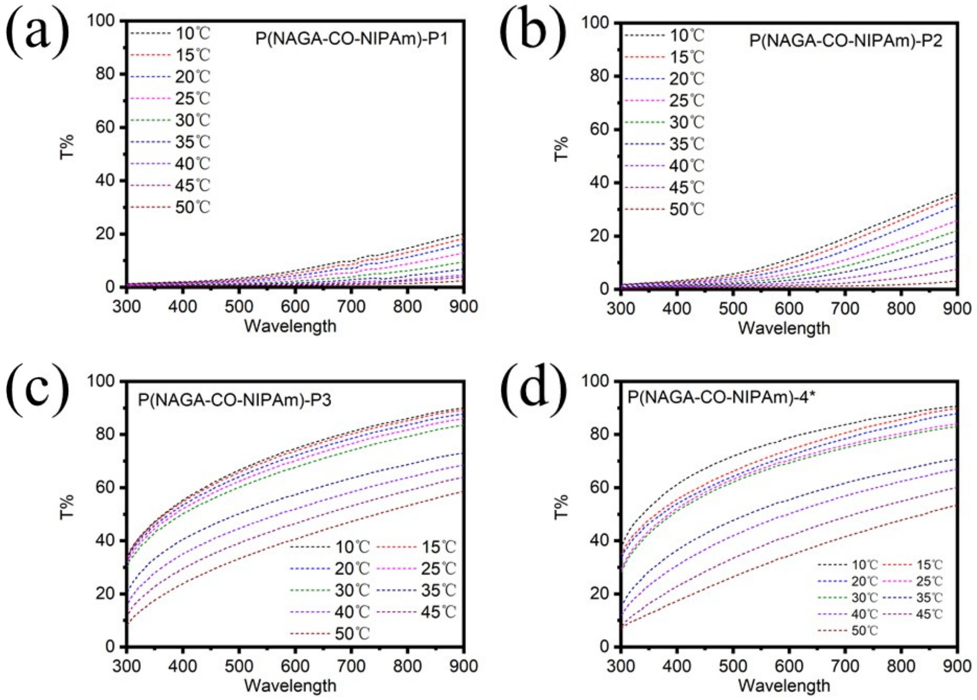

Figure. S5. (a-c) Predicted light transmission curves of P(NAGA-CO-NIPAm)-P1~P3 hydrogels at different temperatures, (d) the transmittance profile of P(NAGA-CO-NIPAm)-4* corresponds to the predicted value of P(NAGA-CO-NIPAm)-P3.

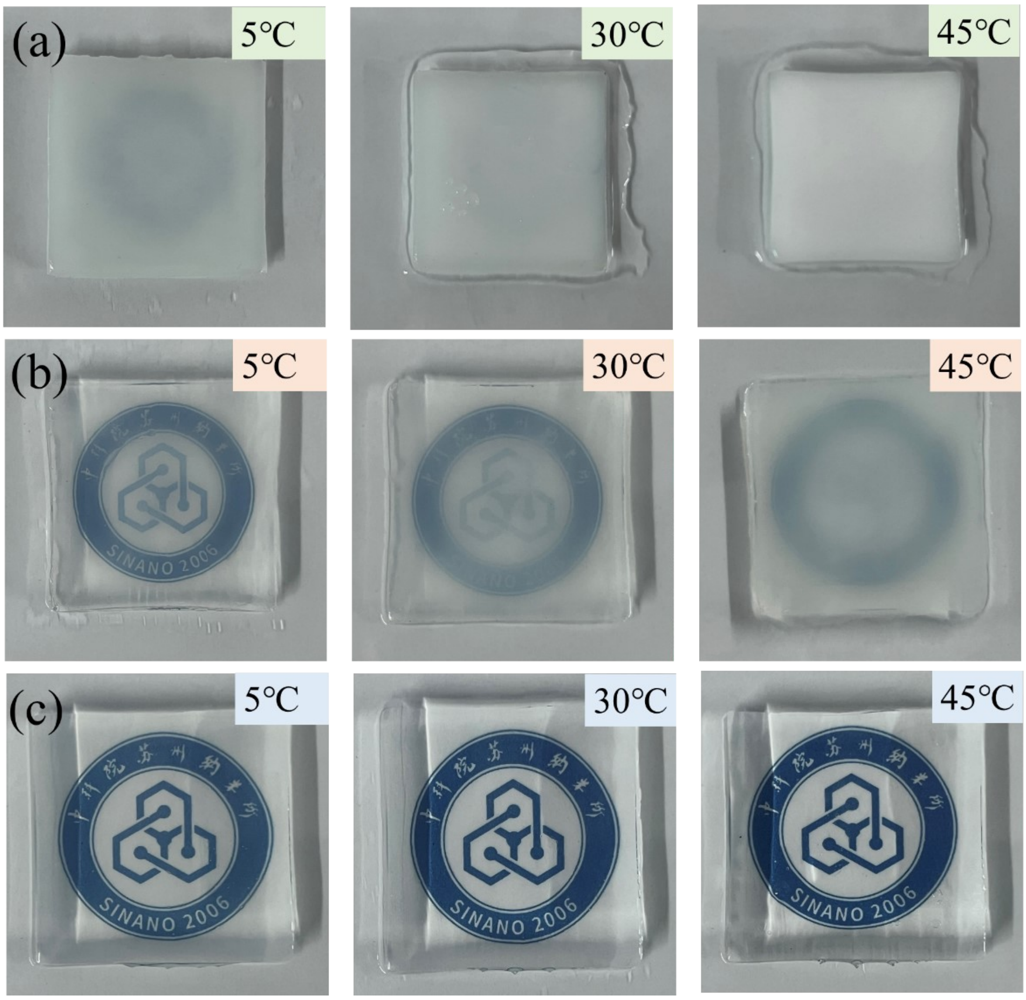

Figure. S6. Physical diagram of (a) P(NAGA-CO-NIPAm)-1, (b) P(NAGA-CO-NIPAm)-4* and (c) P(NAGA-CO-NIPAm)-5 hydrogel phase change losing water at 5 °C, 30 °C and 45 °C for 5 min.

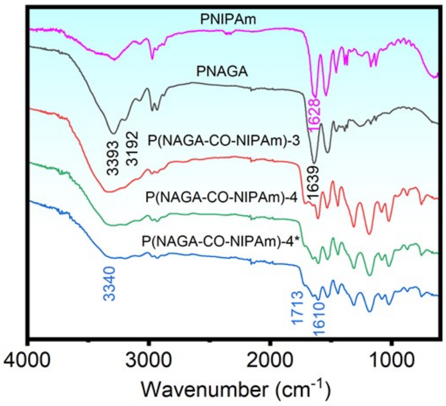

Figure. S7. FTIR spectra of PNIPAm, PNAGA, P(NAGA-CO-NIPAm)-3, P(NAGA-CO-NIPAm)-4, and P(NAGA-CO-NIPAm)-4*.

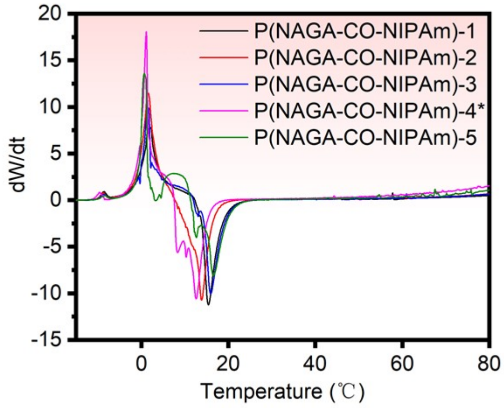

Figure. S8. The DSC derivation of P (NAGA-CO-NIPAm) hydrogels

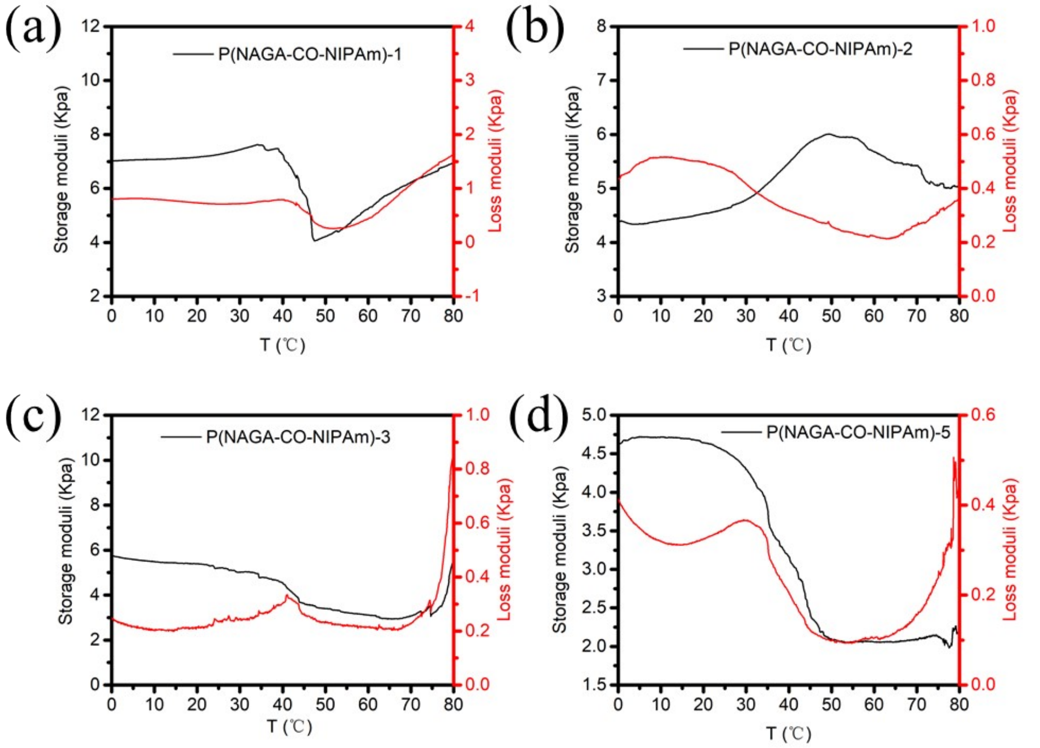

Figure. S9. Storage modulus and loss modulus of P(NAGA-CO-NIPAm)-1, P(NAGA-CO-NIPAm)-2, P(NAGA-CO-NIPAm)-3, and P(NAGA-CO-NIPAm)-5 hydrogels.

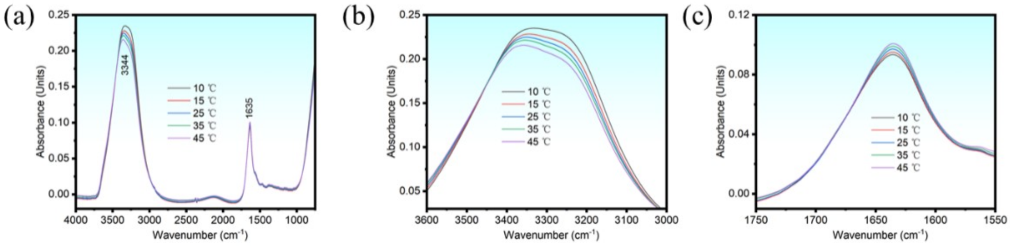

Figure. S10. The situ variable-temperature FTIR spectroscopy of P(NAGA-CO-NIPAm)-4* hydrogel at different temperatures (10, 15, 25, 35, 45℃).

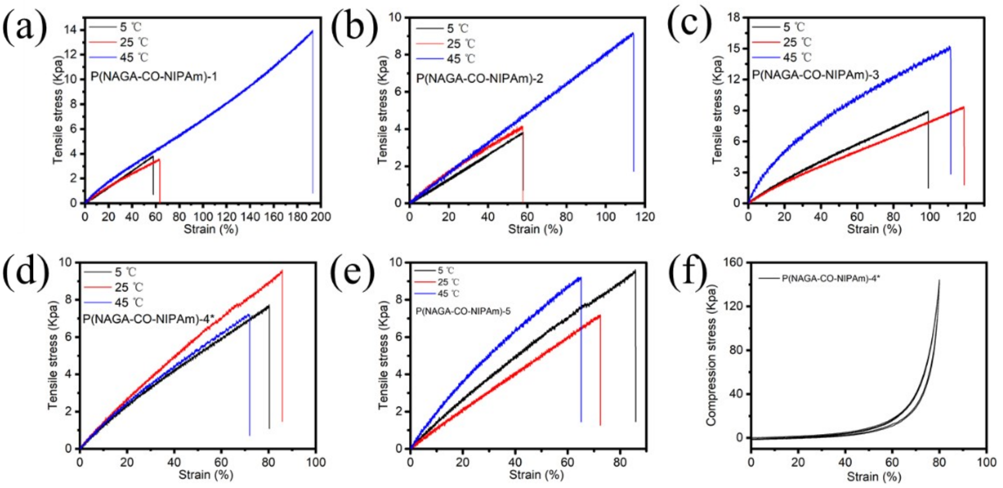

Figure. S11. Tensile strength of P(NAGA-CO-NIPAm)-1 (a), P(NAGA-CO-NIPAm)-2 (b), P(NAGA-CO-NIPAm)-3 (c), P(NAGA-CO-NIPAm)-4* (d) and P(NAGA-CO-NIPAm)-5 (e) at 5℃, 25℃ and 45℃. (f) P(NAGA-CO-NIPAm)-4* cyclic tensile responses at 80% stretch for 50 cycles after removing the initial number of hysteresis.

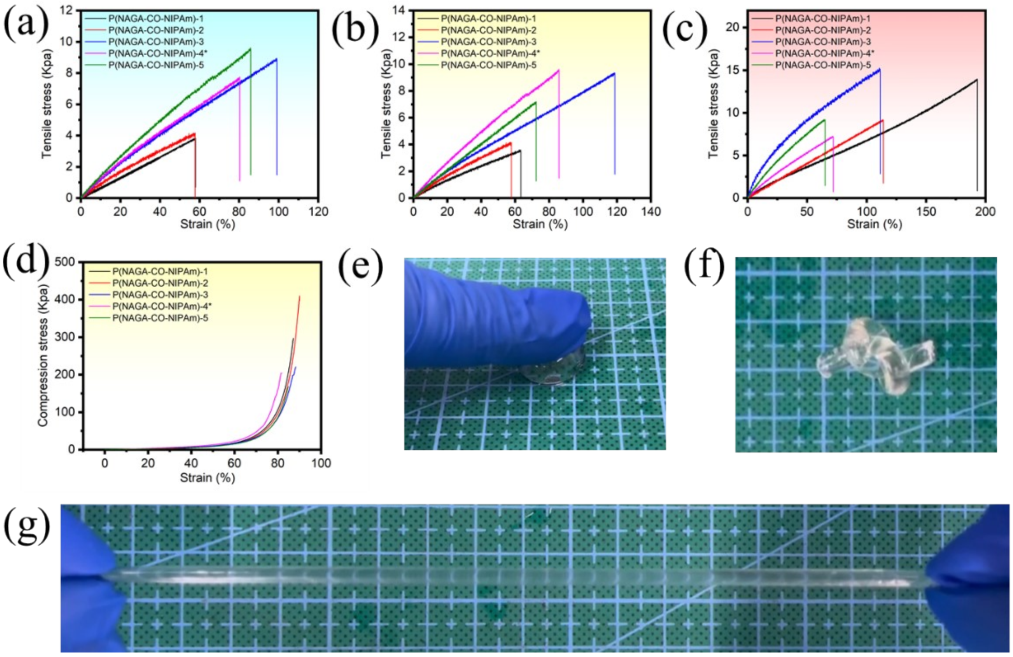

Figure. S12. Tensile strength of P(NAGA-CO-NIPAm) at 5℃ (a) ,25℃ (b) and 45℃ (c). (d) Compressive strength of P(NAGA-CO-NIPAm) temperature-sensitive hydrogels. Physical photograph of P(NAGA-CO-NIPAm)-4* withstanding compression (e), kinking (f), and stretching (g).

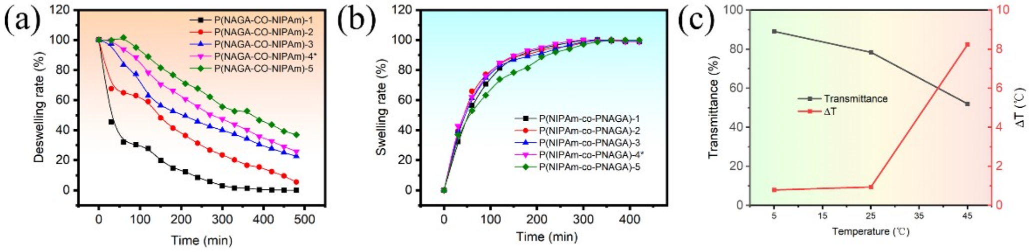

Figure. S13. (a) Deswelling rate curve of P(NAGA-CO-NIPAm) hydrogel at 60 °C; (b) Swelling rate curve of P(NAGA-CO-NIPAm) hydrogel at room temperature; (c) Trend plots of P(NAGA-CO-NIPAm)-4* hydrogel's transmittance and cooling properties with increasing temperature under , 200 W/m^2 radiation.

Figure. S14. Schematic diagrams of the original (a), evaporative (b) and hybrid (c) refrigeration states for passive refrigeration simulation

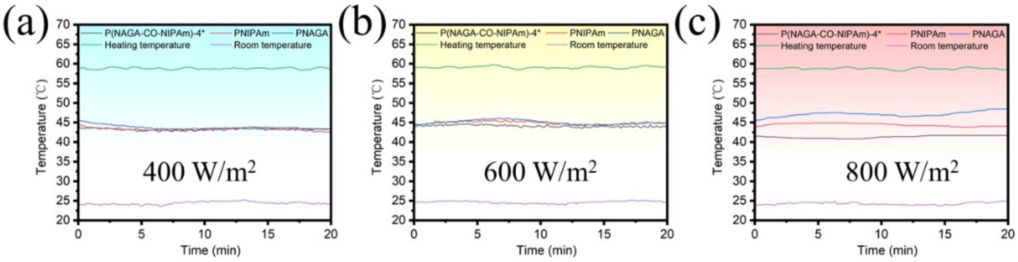

Figure. S15. Hybrid cooling performance of P(NAGA-CO-NIPAm)-4*, PNIPAm, and PNAGA hydrogel at 60 °C for 15 min at 400 W/m^2 (a); 600 W/m^2 (b) and 800 W/m^2 (c).

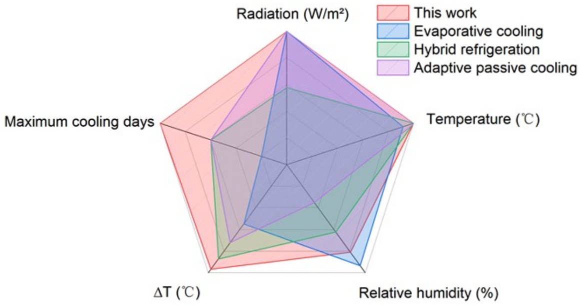

Figure. S16. Comparison on typical properties (cooling change temperatures and maximum cooling days actually) of evaporative cooling, [33, 53] hybrid refrigeration, [3, 54, 55] adaptive passive cooling[15,27] and this work under similar extreme conditions (radiation, temperature, relative humidity).